Dynamics of Kink Bands in Layered Liquids: Theory and in Situ SAXS Experiments on a Block Copolymer Melt

Lei Qiao,[†] Karen I. Winey,*[,†] and David C. Morse*[,‡]

Laboratory for Research on the Structure of Matter, Department of Materials Science & Engineering, University of Pennsylvania, Philadelphia, Pennsylvania 19104-6272, and Department of Chemical Engineering & Materials Science, University of Minnesota, Minneapolis, Minnesota 55455

Received April 9, 2001; Revised Manuscript Received July 20, 2001

ABSTRACT: We consider the dynamics of an isolated kink band within an otherwise well-aligned lamellar block copolymer (or other smectic A liquid crystal) subjected to a macroscopic shear flow. We find on geometrical grounds that normal relative motion of the tilt boundaries that delineate such a band, relative to the normal velocity of the fluid, can occur only if there is jump in the tangential component of the fluid velocity across the boundary. We show that such tangential slippage should be negligible for well-developed bands with narrow boundaries. These observations lead to a simple description of the evolution of an idealized kink band, in which the kink bandwidth remains constant after the formation of narrow tilt boundaries, and the tilt boundaries rotate as material surfaces in a shear flow. The resulting prediction for the rate of rotation of the layers within such a band is confirmed by in situ small-angle X-ray scattering (SAXS)-steady shear experiments, which measure the evolution of the distribution of lamellar orientations within kink bands in a predominantly parallel poly(styrene-*co*-ethylenepropylene) diblock copolymer.

Introduction

Block copolymers can form a variety of microphase-separated morphologies, depending on the volume fraction, the total molecular weight, and the interaction parameter. Laboratory research and industrial applications involving these nano-structured morphologies often employ large-scale alignment through the application of external flow fields, such as oscillatory shear, steady shear, extrusion, or injection. During these alignment processes, defect control and elimination are critical in order to achieve optimum global orientation of the morphology.

Experimental and theoretical efforts to understand defects have focused both on the structure of defects, such as grain boundaries[1−3] and, to a lesser extent, on the response of such defects to mechanical deformation.[4−8] Our group has systematically studied a particular type of transient defect, kink bands, which can appear during the alignment process.[6−8] Kink bands are prevalent in lamellar diblock copolymers and are the origin of the previously observed parallel-transverse biaxial texture.[9] The structure of an idealized kink band is shown in Figure 1. A kink band is defined by a pair of parallel, but opposite tilt boundaries,[6] across which the lamellae bend but remain continuous, between which lies a region of flat parallel lamellae in which the lamellar normal is misaligned by some tilt angle μ from that in the surrounding matrix. The width ξ of a single tilt boundary (i.e., the distance over which the lamellae bend) is typically of the order of a few lamellar spacings and tends to decrease with increasing tilt angle.[1] In contrast, the kink band width W (i.e., the distance between the two opposite tilt boundaries) is much larger, typically 0.5−1 μm.[7,8]

Oscillatory shear and steady shear have been shown to create kink bands in initially well-aligned parallel lamellar block copolymer melts.[6,7,9] Electron microscopy (field-emission SEM and TEM) has been used to examine the kink band morphologies and their evolution with deformation. Polis and co-workers investigated the initiation and evolution of kink bands during shear, at strains less than 1, and concluded that kink bands form from preexisting defects or regions of slight misorientation and sharpen into well-defined kink bands, with tilt boundaries of width $\xi \ll W$, only above a critical strain.[6,7] A subsequent study by Qiao et al. [8] involving larger steady strains of 1−10 strain units provided clear evidence for rotation of the lamellae within kink bands toward the shearing direction. In addition, large strains were found to induce morphological transformations of the tilt boundaries from the chevron type boundary, to the omega boundary, and to broken lamellae at the boundary. These transformations provide a mechanism for the elimination of kink bands at very large strains.

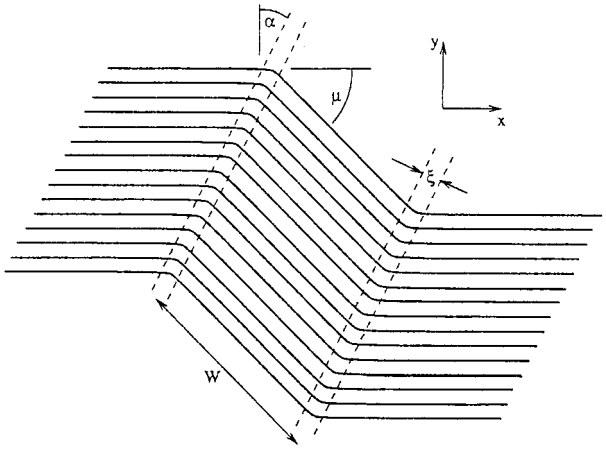

Figure 1. Schematic of an idealized kink band, in which a region of misaligned parallel lamellae of width W is separated from perfectly aligned matrix regions by two long, parallel tilt boundaries, each of width $\xi \ll W$. We consider a situation in which the matrix is subjected to shear flow along the layers in the x-direction.

[†] University of Pennsylvania.
[‡] University of Minnesota.
* To whom correspondence should be addressed.

10.1021/ma010611r CCC: $20.00
Published on Web 09/20/2001

The width of kink bands appears to remain approximately constant during their evolution, since an average width of 0.5−1 μm was found at all strains and rates studied.[7,8]

The ex situ electron microscopy results summarized above provide information with regard to the morphology of kink bands as well as slices of dynamic information during kink band evolution. In situ small-angle X-ray scattering (SAXS) provides complementary information about the dynamic evolution of the system, by probing the evolution of the distribution of lamellar orientations. A previous study using simultaneous in situ SAXS and rheological measurements focused on the evolution of the main scattering peak during steady shear, which arises from scattering from the predominantly parallel matrix, and identified a slight rotation of the maximum of this main peak in a direction opposite to the vorticity of the flow. This counter-rotation of the scattering maxima was explained by considering a population dynamics model for the matrix material, in which different regions of the nearly aligned matrix are assumed to rotate with the vorticity of the flow, but with an orientation-dependent rotational velocity that is assumed to vanish for perfectly aligned lamellae.[10] That study also reported the existence of a distinct secondary peak that sharpens and separates from the main peak with increasing strain, which we believe to arise from scattering from kink bands. The current study explores the evolution of this secondary peak, in a sample that has been prepared with a large population of preexisting kink bands, in which this secondary peak is better defined. Our analysis of the evolution of this peak with time or strain makes use of a model for the evolution of the underlying population of kink band orientations, which are assumed to rotate at a rate predicted by a simple mechanical model for the motion of a single idealized kink band in shear flow. The paper will be presented in four parts: a theory of kink band dynamics, in situ SAXS rheology results, comparison of theory and experiment, and discussion of the results.

Theory

Here we present a model for the evolution of the orientation and width of a single kink band within an otherwise well-aligned lamellar phase. The matrix material on either side of the kink band is subjected to shear flow with fluid velocity along the x-axis and a velocity gradient along the y-axis, with a lamellar normal that remains parallel to the y-axis. We consider only the late stages of evolution, after the formation of a well-defined kink band with narrow tilt boundaries. We consider an idealized geometry (Figure 1) in which a kink band is viewed as a strip of misaligned material of width $W(t)$ within which the layers remain straight and parallel but are tilted by an angle $\mu(t)$ from the orientation in the two surrounding matrix regions. The kink band is separated from the matrix regions by a pair of narrow, parallel tilt boundaries, which are tilted by an angle $\alpha(t)$ from the y-axis. The lamellar layers are assumed to remain continuous through both tilt boundaries, as observed in electron microscopy at modest strains. The tilt boundaries will be treated for most purposes as mathematical surfaces across which the layer orientation, fluid velocity, and stress may change discontinuously but are actually narrow regions, of width $\xi \ll W(t)$, within which these quantities exhibit large gradients. The width and shape of a low angle chevron tilt boundary may be predicted by minimizing the smectic A elastic energy appropriate for a layered liquid,[2,11] which yields a width of order $\xi \approx \sqrt{K/B}\mu^{-3}$, where K and B are bending and compression moduli and $\sqrt{K/B}$ is a smectic penetration length that is typically on the order of a lamellar spacing in block copolymers.

For simplicity, we will initially ignore the slight flow-induced changes in layer spacing observed in experiment (typically $<4\%$)[12,13] and assume that the layer spacing stays equal to its equilibrium value D_0 throughout both the matrix and the body of the kink band. The assumption of constant layer spacing, when combined with the assumption of continuous layers, requires that the tilt boundaries bisect the angle between the layer normals in the kink band and matrix regions and thus that $\alpha(t) = \mu(t)/2$. Relaxing this last assumption can be shown to lead to only slight changes in the predicted rate of lamellar rotation.

To establish the relationship between the fluid velocity field in and around a kink band and the evolution of the layer positions (i.e., as described by either a composition field or height fields for the layers), we assume that there is negligible permeation in the systems of interest: We assume that the normal velocity of a layer (as defined by, e.g., a surface of constant chemical composition) is equal to the projection of the fluid velocity onto the direction normal to the layers, so that there is no net flow of material from one layer to the next.

Mass and Force Balance along a Tilt Boundary. First, consider the boundary conditions that relate the fluid velocity and stress field on either side of one of the two kink boundaries. For specificity, we focus on the boundary that separates the kink band from the matrix material to its left (i.e., smaller x). The analysis of the other tilt boundary in a symmetric tilt band is similar, aside from some changes of sign. Let the fluid velocities within the matrix and kink band be denoted by $\mathbf{v}_{\mathrm{matrix}}(\mathbf{r})$ and $\mathbf{v}_{\mathrm{kink}}(\mathbf{r})$, respectively, and the corresponding stress tensors by $\tau_{\mathrm{matrix}}(\mathbf{r})$ and $\tau_{\mathrm{kink}}(\mathbf{r})$. Conservation of mass and momentum along the tilt boundary requires that the normal components of the velocity and stress remain continuous across the tilt boundary, i.e.

$$0 = \hat{\mathbf{n}} \cdot (\mathbf{v}_{\mathrm{matrix}} - \mathbf{v}_{\mathrm{kink}}) \tag{1}$$

$$0 = \hat{\mathbf{n}} \cdot (\tau_{\mathrm{matrix}} - \tau_{\mathrm{kink}}) \tag{2}$$

everywhere along the boundary, where $\hat{\mathbf{n}} = \cos(\alpha)\hat{\mathbf{x}} - \sin(\alpha)\hat{\mathbf{y}}$ is a unit vector normal to the tilt boundary.

Tilt Boundary Migration. We next consider the relationship between motion of the tilt boundary and the fluid velocities in the neighboring regions. Let v_{b} be the velocity at which some point along the left tilt boundary in a kink band is displaced along the normal direction $\hat{\mathbf{n}}$ and $v_{\perp} = \hat{\mathbf{n}} \cdot \mathbf{v}_{\mathrm{matrix}} = \hat{\mathbf{n}} \cdot \mathbf{v}_{\mathrm{kink}}$ be the normal component of the fluid velocity, which must be continuous across the boundary by eq 1. The boundary will be said to migrate if the boundary does not follow the normal fluid velocity, i.e., if $v_{\mathrm{b}} \neq v_{\perp}$.

Our main conclusion is that boundary migration can occur only if there is an apparent discontinuity in the tangential fluid velocity (i.e., tangential slippage) across the kink band. This conclusion may be understood most easily by considering the simple geometry shown in

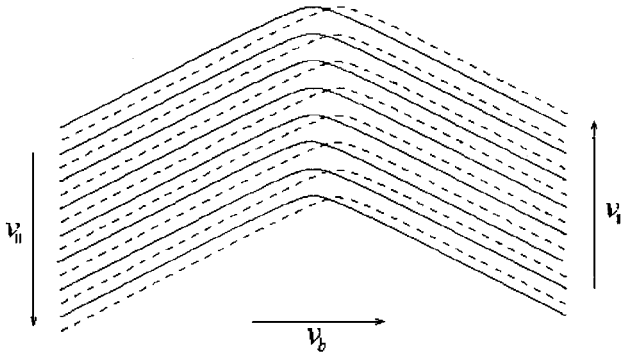

Figure 2. Schematic of a moving chevron tilt boundary and of the relationship between boundary migration and tangential slippage. Dotted lines represent the lamellae at a time slightly later than that represented by the solid lines. Migration of the boundary to the right at a normal velocity v_b causes the neighboring regions to move tangentially (i.e., vertically) at equal but opposite rates $\pm v_{||}$ in order to maintain layer continuity.

Figure 2, in which a single symmetric chevron tilt boundary is oriented along the *y*-axis, with layers tilted by angles $\pm\alpha$ from the *x*-axis. The boundary undergoes uniform migration along the *x*-axis, in the absence of any fluid flow in the normal direction (i.e., $v_\perp = 0$). If one imagines sliding the boundary between the two domains to the right, it is clear that it is necessary to translate layers to the right side of the boundary up and those to the left of the boundary down in order to maintain layer continuity (compare the solid and dotted lines in Figure 2). This requires an essentially discontinuous change in the tangential (i.e., vertical) velocity across the tilt boundary. This situation is more general than it might appear, since any tilt boundary can be made to look like this one by viewing it from a frame of reference that rotates with the boundary (so that the boundary remains aligned along the *y* axis), translates along the direction normal to the boundary with a velocity equal to the normal component of the fluid velocity (so that there is no fluid flow along the *x*-axis in this frame of reference), and translates along the boundary with a velocity chosen so that the tangential velocities of the two domains just outside the tilt boundary are equal and opposite.

A more detailed analysis may be given, in this same frame of reference, by describing the *n*th layer in such a symmetric chevron by a height field $y = h_n(x)$, such that $d^2h_n(x)/dx^2 \neq 0$ only within a tilt boundary of width ξ and such that $dh_n(x)/dx = \mp \tan(\alpha)$ far from the tilt boundary, in the limits $x = \pm\infty$. Neighboring layers must be offset by a distance $D_0 \sec(\alpha)$ along the *y*-axis in order to maintain a normal layer spacing D_0 far from the tilt boundary, giving height fields of the form

$$h_n(x) = f(x) + nD_0 \sec(\alpha) + \text{const} \qquad (3)$$

Here, $f(x)$ is a function that describes the shape of a layer in and near a tilt boundary, which must have constant slopes $df/dx = \mp\tan(\alpha)$ far outside the boundary. The equilibrium chevron shape can be calculated for low-angle boundaries (neglecting any distorting effects of nonequilibrium stress) by minimizing the smectic A elastic free energy subject to the conditions that $df/dx = \mp\tan(\alpha)$ for $x = \pm\infty$.[2,11] Rigid translation of this chevron pattern along the *x*-axis with a velocity v_b may be described by a corresponding set of time-dependent height fields

$$h_n(x,t) = f(x - v_b t) + nD_0 \sec(\alpha) + \text{const} \qquad (4)$$

Differentiating eq 4 with respect to time yields a vertical (i.e., tangential) velocity

$$v_{||}(x,t) = \frac{\partial h_n}{\partial t} = -\frac{\partial f(x - v_b t)}{\partial x} v_b \qquad (5)$$

which depends on the distance $x - v_b t$ from the tilt boundary but which is the same for all layers. At points outside of the tilt boundary, where $\partial f/\partial x = \pm\tan(\alpha)$, this yields tangential velocities

$$v_{||} = \pm\tan(\alpha) v_b \qquad (6)$$

yielding an apparent discontinuity

$$\Delta v_{||} = 2\tan(\alpha) v_b \qquad (7)$$

in the tangential velocity across the tilt boundary. Equation 7 tells us that the rate of normal boundary migration v_b is directly proportional to the rate of tangential slippage $\Delta v_{||}$.

The same conclusion may be obtained, without invoking a special frame of reference, by considering a simple geometrical model in which the lamellae within the matrix region just to the left of the tilt boundary are represented by a set of evenly spaced horizontal lines, and the lamella within the kink band are represented by another set of such evenly spaced lines that are tilted away from those in the matrix by an angle μ. The tilt boundary is then simply the locus of points in the $x-y$ plane where the lines representing the layers in the matrix intersect the corresponding set of lines representing the layers within the kink band, which lie along a line that bisects the angle between the layer normals in the matrix and kink band regions. To describe the motion of a tilt boundary, we may calculate the normal component of the velocity of the point of intersection at which some layer passes through the tilt boundary (viewed here as a mathematical surface), while assuming that the layers in both regions are displaced along their local layer normal direction with a velocity equal to the normal component of the local fluid velocity. It is straightforward to show by this method that the relative normal velocity of the boundary is given by

$$v_b - v_\perp = \frac{\Delta v_{||}}{2\tan(\alpha)} \qquad (8)$$

where $\Delta v_{||} = \mathbf{t}\cdot(\mathbf{v}_{\text{kink}} - \mathbf{v}_{\text{matrix}})$ is the rate of tangential slippage and $\hat{\mathbf{t}} = \cos(\alpha)\hat{\mathbf{y}} + \sin(\alpha)\hat{\mathbf{x}}$ is a unit vector constructed tangential to the tilt boundary. Equation 8 is simply the generalization of eq 7 to an arbitrary frame of reference, with a nonzero normal fluid velocity.

Tangential Slip. To describe the motion of the kink band boundary or to obtain a well-posed problem for the fluid velocity, we must thus specify a boundary condition for the tangential components of velocity along either kink boundary. In normal fluid mechanics, this is usually taken to be a no-slip boundary condition. Here, we allow for the possibility of tangential slip along the boundary (i.e., a rapid change over a distance of order the tilt boundary thickness ξ) but assume that the magnitude of any discontinuity in tangential velocity will be proportional to the magnitude of the tangential

force applied along the boundary, which would tend to drive slippage. We thus assume a linear relationship of the form

$$\varsigma \Delta v_{\|} = f_{\|} \tag{9}$$

where ς is a phenomenological friction coefficient, $\Delta v_{\|} = \hat{\mathbf{t}}\cdot(\mathbf{v}_{\text{kink}} - \mathbf{v}_{\text{matrix}})$ and

$$f_{\|} \equiv \hat{\mathbf{n}}\cdot\tau_{\text{matrix}}\cdot\hat{\mathbf{t}} = \hat{\mathbf{n}}\cdot\tau_{\text{kink}}\cdot\hat{\mathbf{t}} \tag{10}$$

is the tangential force per area exerted by the kink band upon the matrix across the boundary.

If we assume that the narrow strip of material within the tilt boundary may be characterized by an effective viscosity η, then we obtain a friction coefficient

$$\varsigma \approx \eta/\xi \tag{11}$$

If the effective viscosity is roughly independent of the boundary width ξ, the friction coefficient ζ will diverge in the limit of narrow tilt boundaries, because, for a given apparent discontinuity in tangential velocity, the actual shear rate within the tilt boundary must increase as the width ξ of the boundary region is decreased. The shear stress within the tilt boundary must be equal to the tangential component $\hat{\mathbf{n}}\cdot\tau\cdot\hat{\mathbf{t}}$ of the stress in the neighboring matrix or kink band domain, which will typically be the same order of magnitude as the bulk shear stress. If the effective viscosity within the tilt boundary is of the same order of magnitude as the bulk viscosity, then the typical rate of shear within the tilt boundary will be of the same order of magnitude as that in the matrix. This would lead to an apparent discontinuity in the tangential velocity of roughly $\Delta v_{\|} \approx \dot{\gamma}\xi$ and to a relative tilt boundary velocity $v_b - v_\perp$ of the same order of magnitude, except in the limit of very low-angle tilt boundaries. Normal boundary velocities of this magnitude would have a negligible effect upon the changes in the kink band orientation and width in the limit $\xi \ll W$ of interest, since, at this velocity, it would take a time of order $W/(\dot{\gamma}\xi)$, or a macroscopic strain $W/\xi \gg 1$, to translate a boundary a distance comparable to the tilt boundary width W. We thus conclude that there should be negligible tangential slip along a tilt boundary in the limit of well-defined kink bands. A no-slip boundary condition

$$\mathbf{v}_{\text{matrix}} \approx \mathbf{v}_{\text{kink}} \tag{12}$$

should therefore remain approximately valid in this limit.

The conclusions that (1) tilt boundary migration requires tangential slippage and (2) slippage should be negligible in the limit of narrow boundaries together imply that there should be negligible tilt boundary migration in this limit. In the absence of this conclusion, a kink band bounded by two parallel tilt boundaries might be thought to undergo some combination of a homogeneous change in width, corresponding to a normal boundary velocity that is uniform along each boundary and/or a rotation of the kink band boundary relative to the fluid, corresponding to a relative normal boundary velocity that varies linearly along the length of each tilt boundary. Both types of motion are instead ruled out. The conclusion that the kink bandwidth should not change substantially after the formation of narrow boundaries is consistent with previous electron microscopy observations.[7,8]

The possibility of a relative rotation of the tilt boundary can actually be ruled out without relying on the above arguments about the magnitude of tangential slip, as follows: Relative rotation of the kink boundary would be described by a relative normal boundary velocity that varies linearly with distance along the boundary. By eq 6, this would require a tangential discontinuity that also varies linearly along the tilt boundary. By eq 3, this would in turn require a stress that varies linearly along the boundary. None of this is consistent with the picture of a long kink band as a region with a nearly uniform stress and velocity gradient. Allowing for a nonnegligible tangential slippage along a tilt boundary between two regions with homogeneous stress fields (by, e.g., postulating a much lower effective viscosity within the tilt boundary than in the matrix) thus would actually not, by itself, change our conclusions regarding the rate of boundary rotation, though it would cause the kink bandwidth to change with time.

Rotation of an Idealized Kink Band. In the idealized kink band geometry shown in Figure 1, we approximate the fluid velocity $\mathbf{v}_{\text{matrix}}(\mathbf{r})$ in either of the two matrix regions as simple shear flow, of the form

$$\mathbf{v}_{\text{matrix}}(\mathbf{r}) = \mathbf{v}_{\text{m},0} + \dot{\gamma}\hat{\mathbf{x}}\hat{\mathbf{y}}\cdot\mathbf{r} \tag{13}$$

in which $\dot{\gamma}$ is the macroscopic shear rate, and $\mathbf{v}_{\text{m},0}(\mathbf{r})$ is a constant velocity that depends on one's choice of spatial origin and frame of reference and that may be different for the two matrix regions.

The conclusion that the tilt boundary cannot move relative to the fluid in the direction normal to the boundary implies that each tilt boundary must rotate as a material surface in the simple shear flow of the adjoining matrix region, i.e., that a tilt boundary exhibits the same rotation law as a straight line of ink drawn in a shear flow. This may be shown to yield a rate of rotation

$$\dot{\alpha} = \dot{\gamma}\cos^2(\alpha) \tag{14}$$

for the tilt boundaries, which is equivalent to the rate of rotation of an infinitely thin non-Brownian rigid rod in a shear flow. This is equivalent to a rate of rotation

$$\dot{\mu} = \dot{\gamma}\, 2\cos^2(\mu/2) \tag{15}$$

for lamellae within the kink band. Note that the rate of rotation decreases monotonically from a maximum value at $\mu = 0$ and vanishes when $\mu = \pi$.

By integrating eq 15 with respect to time, from the onset of shearing at $t = 0$ to an arbitrary time t, we may show that the orientation μ at time t of a kink band that had an initial orientation μ_0 at time $t = 0$ satisfies the equation

$$\tan\left(\frac{\mu}{2}\right) - \tan\left(\frac{\mu_0}{2}\right) = \dot{\gamma}t \tag{16}$$

Note that in the limit $\dot{\gamma}t \gg 1$ of large strain $\tan(\mu/2)$ must diverge, and so μ approaches π, independent of the initial orientation μ_0. The effect of rotation law eq 14 is thus to cause all kink bands to asymptotically approach the doubled-over orientation with $\mu = \pi$, where the rate of rotation eq 15 vanishes. The SAXS experiments described below provide a direct test of eqs 15 and 16.

Reversal of Shear within a Kink Band. To describe the flow field $\mathbf{v}_{kink}(\mathbf{r})$ within the kink band, we assume a purely two-dimensional flow with a spatially homogeneous velocity gradient tensor. This assumption, when combined with the assumptions of negligible permeation, constant layer spacing (which rules out uniaxial extension along the local layer normal), and fluid incompressibility, is sufficient to constrain the fluid velocity within the kink band to be a combination of rigid translation, rigid rotation, and shear flow along the layers, i.e.,

$$\mathbf{v}_{kink}(\mathbf{r}) = \mathbf{v}_{kink,0} - \dot{\mu}\hat{\mathbf{z}} \times \mathbf{r} + \dot{\gamma}_{kink}\hat{\mathbf{l}}\,\hat{\mathbf{m}}\cdot\mathbf{r} \qquad (17)$$

where $\mathbf{v}_{kink,0}$ is the rate of rigid translation, $\dot{\gamma}_{kink}$ is the rate of shear within the kink band, $\hat{\mathbf{z}} = \hat{\mathbf{x}} \times \hat{\mathbf{y}}$ is unit normal along the vorticity axis, and $\hat{\mathbf{m}} = \cos(\mu)\hat{\mathbf{y}} + \sin(\mu)\hat{\mathbf{x}}$ and $\hat{\mathbf{l}}(t) = \hat{\mathbf{m}}(t) \times \hat{\mathbf{z}}$ are unit vectors constructed normal and parallel to the layers within the kink band, respectively. By substituting eqs 13 and 17 for the fluid velocities into mass balance eq 1 and differentiating the result with respect to distance along the kink band, we find that the rates of rotation and shear within the kink band and matrix must satisfy a corresponding constraint

$$\dot{\mu}(t) = [\dot{\gamma} - \dot{\gamma}_{kink}(t)]\cos^2(\mu(t)/2) \qquad (18)$$

in order to avoid accumulation or depletion of material along either tilt boundary. Comparing this to eq 15 for the rate of rotation, we see that

$$\dot{\gamma}_{kink} = -\dot{\gamma} \qquad (19)$$

i.e., the rate of shear inside the kink band must be equal in magnitude but *opposite* in sign from that in the surrounding matrix.

This observation leads to a simple picture of the rotation of a kink band, which may be visualized as follows: Imagine that we represent the kink band and surrounding matrix by three decks of cards: one representing the matrix to the left of the kink band, one representing the kink band, and one representing the matrix to the right of the kink band. Imagine that each card in the middle (kink band) deck is connected by a flexible hinge (i.e., a piece of tape) at one end to a corresponding card from the left deck and at the other to a corresponding card in the right deck. The motion described above is that which is obtained if we deform the resulting structure so as to keep the left- and rightmost decks parallel to some solid surface (i.e., a table or a rheometer plate), while subjecting these two decks to steady shear (sliding of neighboring cards over one another), and lifting the left deck so as to allow rotation of the middle (kink band) deck of cards. As the angle between the kink band deck and either of the two neighboring decks increases, the kink band deck must shear in a sense opposite to that of the two matrix decks in order to prevent a depletion of material at the top of the deck and an accumulation of material at the bottom along the left tilt boundary or an accumulation of material at the top of the deck and a depletion at the bottom along the right boundary. The point at which a continuous lamella layer (represented here by three taped cards) passes through a tilt boundary always remains at the same material point along the lamellae (corresponding to a point at which the cards are attached by a flexible hinge), rather than migrating to some other point along the layer (thus forcing one of the cards to bend) because of the absence, in the real system, of any significant boundary migration. This simple folding motion appears to be the only one possible for a system with narrow parallel tilt boundaries and negligible boundary migration.

The fact that the model predicts a reversal of the rate of shear within a kink band is one indication that it cannot describe the early stages of the evolution of a kink band. Electron microscopy studies have suggested that kink bands have less sharply defined S-shaped regions in their initial stage. At the onset of steady strain, we expect the local rate of shear to have the same sign throughout any such slightly deformed region. There must therefore be an initial stage of the evolution of a kink band during which initially diffuse curves sharpen into pairs of narrow chevron boundaries and the rate of shear must reverse sign within the newly formed kink band. The model described here is intended to describe only the later stages of evolution, after narrow boundaries form.

Stress within a Kink Band. We can use the force balance eq 2 to relate the state of stress inside a kink band to that in the matrix. The local stress inside a kink band is not directly measurable but is indirectly related to the slight changes in layer spacing. We assume that the stress in the adjoining matrix and kink band domains may be expressed as sums

$$\tau_{matrix} = -p_{matrix}\mathbf{I} - \Pi_{matrix}\hat{\mathbf{y}}\hat{\mathbf{y}} + \sigma_{matrix}(\hat{\mathbf{x}}\hat{\mathbf{y}} + \hat{\mathbf{x}}\hat{\mathbf{y}}) \qquad (20)$$

$$\tau_{kink} = -p_{kink}\mathbf{I} - \Pi_{kink}\hat{\mathbf{m}}\hat{\mathbf{m}} + \sigma_{kink}(\hat{\mathbf{l}}\,\hat{\mathbf{m}} + \hat{\mathbf{m}}\hat{\mathbf{l}}) \qquad (21)$$

of hydrostatic pressures p_{matrix} and p_{kink}, uniaxial compressive stresses Π_{matrix} and Π_{kink} that act along the local layer normals, and shear stresses σ_{matrix} and σ_{kink} with tensor components also defined relative to the local layer orientations.

Substituting these expressions for the stress into the force balance, and decomposing the resulting vector into components normal and tangential to the tilt boundary, yields two conditions relating the six variables used to parametrize the stress. The balance of normal forces, which is obtained by setting $\hat{\mathbf{n}}\cdot(\hat{\tau}_{matrix} - \hat{\tau}_{kink})\cdot\hat{\mathbf{n}} = 0$, is found to contain terms involving the hydrostatic pressures and yields little useful information. The balance of tangential forces, which is obtained by setting $\hat{\mathbf{n}}\cdot(\hat{\tau}_{matrix} - \hat{\tau}_{kink})\cdot\hat{\mathbf{t}} = 0$, does not involve the hydrostatic pressures and yields the following relationship between the uniaxial and shear stress components:

$$\Pi_{matrix} + \Pi_{kink} = -(\sigma_{matrix} - \sigma_{kink})2\cot(\mu) \qquad (22)$$

The matrix shear stress σ_{matrix} is expected to be positive. We showed above that a well-developed kink band actually experiences a rate of shear opposite to that in the matrix. If molecular relaxation rates are large compared to the macroscopic shear rate, so that the local shear stress depends only on the current local rate of shear, the shear stress in the kink region will thus also be equal and opposite to that in the matrix. More generally, we expect the reversal of the direction of shear within the kink band after the formation of narrow tilt boundaries to either change the sign of the shear stress in the kink band or at least decrease its magnitude, and so we expect the quantity $\sigma_{matrix} - \sigma_{kink}$

to always be positive. Equation 20 thus implies that, to establish a balance of tangential forces along a tilt boundary, either the matrix or the tilt boundary, or both, must experience a uniaxial tension (i.e., $\Pi < 0$). If the boundary conditions on the matrix are such that it can support little or no uniaxial tension, then the kink band must be under tension.

Note that the tensile stress predicted by eq 22 increases with decreasing μ and actually diverges in the limit $\mu = 0$ of a flat kink band. This, like the predicted reversal of shear within a kink band, is another indication that our model of a well-defined kink band with narrow boundaries cannot be used to describe the initial stages in the growth of a kink band.

Experimental Methods

Materials. The polymer used in this study was a lamellar poly(styrene-*b*-ethylenepropylene) diblock copolymer. It has a weight-averaged molecular weight, M_w, of 100 000 g/mol (with a polydispersity index of 1.02) and 38 wt % styrene monomeric unit content and will be referred to as SEP(38-62), corresponding to the nominal molecular weights of the PS and PEP blocks. Details regarding polymerization and molecular weight characterization of this block copolymer can be found elsewhere.[10] Approximately 1 mm thick films of SEP(38-62) were cast at room temperature from a 5 wt % toluene solution. The films were dried under vacuum for 24 h at room temperature, followed by 24 h at 120 °C, and annealed at 150 °C for 48 h. The samples were compression-molded at 150 °C for the subsequent oscillatory shear and steady shear experiments. The morphology after annealing and molding is a lamellar structure with a long period of ~70 nm, as determined from small-angle X-ray scattering.

SAXS-Rheology. In situ SAXS rheology experiments were performed on beam line 16.1 of the Synchrotron Radiation Source (SRS) at the Daresbury Laboratory, Warrington, U.K. A Rheometrics Solids analyzer (RSAII), with shear sandwich geometry, was used to prealign the specimen with oscillatory shear and to apply the steady shear deformations. Specially constructed "match-stick" tools were used such that the shearing geometry was rotated 90°, relative to the standard RSAII configuration, to allow for in situ scattering along the neutral direction.[10] The sample dimensions were $12 \times 1 \times 4$ mm^3 along the velocity (1), velocity gradient (2), and neutral (3) direction. A RAPID area detector with 1 μs time resolution was located 3 m from the sample to monitor scattering in the 1*−2* plane. Details regarding monochromation, collimation, detection, and wavelength of the X-rays at beam line 16.1 can be found elsewhere.[14]

The specimen was first sheared at a constant rate of 0.005 s^{-1} to a strain of 80% for half a cycle (forward and back). Large-amplitude oscillatory shear (LAOS) was then used to prealign the specimen in a predominately parallel orientation (1 rad/s, 180 °C, $\gamma = 20\%$ for 20 min, then $\gamma = 40\%$ for 50 min). After annealing the sample for 50 min, steady shear was applied at a series of shear rates, 0.001, 0.01, and 0.1 s^{-1}, to a total strain of 80% for a half cycle while SAXS data were collected. Between each constant shear rate experiment, the sample was annealed for 15−20 min.

Thirty 1-s SAXS patterns were collected in situ at the end of each annealing period, which served as the reference patterns for the starting state. SAXS patterns with either 0.5- or 1-s collection time and 1- or 5-s (for 0.001 s^{-1}) interval between collections were collected in situ during each steady shear deformation, so that the strain resolutions for the three shear rates (0.001, 0.01, and 0.1 s^{-1}) were 0.1%, 0.5%, and 5%, respectively. Azimuthal scans were obtained for the three shear rates by integrating about the second-order Bragg reflection (Figure 3). This is in contrast with earlier data from Polis et al.,[10] which were collected at a sample-to-detector distance of 2 m and obtained by integrating about the fourth-order reflection. The intensity-over-noise ratio is much higher in this study, making it possible to observe the strong rotational phenomena in a single collection frame.

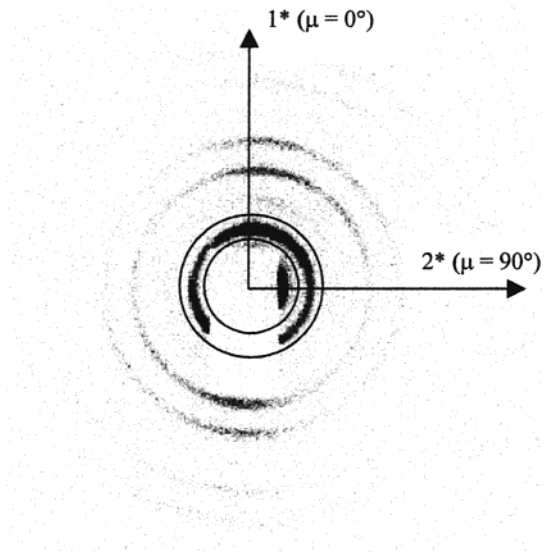

Figure 3. In situ SAXS pattern of the starting state of prealigned SEP(38-62). The X-ray beam was oriented along the 3-direction (perpendicular to the 1−2 plane). Steady shear was along the 1-direction. Azimuthal scans were obtained by integrating about the second-order reflection (area between two concentric circles). The white, rectangular region in the center is the beam stop, which blocks the majority of the first-order reflection and the lower portion of the second-order reflection ($\mu \sim \pm 180°$) and partially obscures the upper left side of the second-order reflection.

FE-SEM. A smooth cross-section of 0.5×0.5 mm^2 in the 1−2 plane of the sample (to image cross-sections of kink bands) was prepared by a Reichert Ultracut cryo-ultramicrotome operated at −100 °C, followed by selectively staining the PS microdomains in a RuO_4 vapor. A Cr coating of ~2 nm thick was evaporated on the sample to reduce charging. A JEOL 6300 FV field-emission scanning electron microscope, operated at ~2 kV, was used to examine the starting state of the sample after LAOS prealignment.

Results

The starting state SAXS pattern at the end of the LAOS procedure ($t = 0$) is shown in Figure 3. Steady shear is along the 1 direction, so that lamellae with normals in the 1−2 plane rotate in the vorticity direction, i.e., the clockwise direction. The white rectangular region at the center of the SAXS pattern is the beam stop that blocks most of the first-order reflection as well as the lower portion of the second-order reflection ($\mu \sim \pm 180°$). The beam stop also partially obscures the upper left side of the second-order reflection, leading to a slightly lower background intensity at $\mu < 0$ (Figure 5). This asymmetric background intensity is not seen in the fourth-order reflection pattern.

Several orders of scattering maxima at 0 and equivalently ±180° were obtained after alignment, indicating a predominately parallel orientation. The intensity distribution has a shoulder to the right of the parallel main peak ($\mu > 0$), as is more evident in subsequent figures at $\gamma = 0$ (Figures 5−7). This off-centered distribution corresponds to a population of forward kink bands in the starting state, as confirmed by ex situ field-emission SEM (Figure 4). These kink bands, created during the initial steady shear before the LAOS procedure (0.005 s^{-1}, 80%, half cycle), have (1) sharp bound-

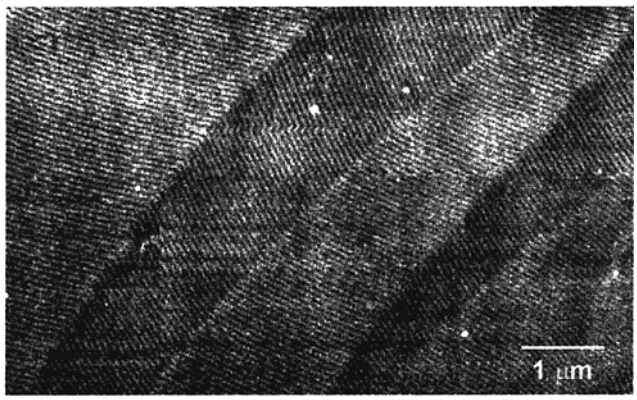

Figure 4. Field emission SEM image of forward kink bands in prealigned SEP(38-62) prior to steady shear. These kink bands, created after steady shear (0.005 s^{-1}, 80%, half cycle at 180 °C) and subsequent LAOS, have sharp boundaries, mostly continuous layers across the boundaries with widths of ~1 μm. The average angle between matrix lamellae and lamellae within kink bands, μ, is ~40°. Note that the orientation of the lamellae in the matrix near these kink bands is not perfectly parallel and in fact slants downward. Separate images of the starting state show the matrix lamellae near kink bands to be in a variety of orientations (upward, downward, and perfectly parallel). The orientation of the matrix as determined by SAXS is more reliable and is predominately parallel.

aries across which layers are mostly continuous, (2) narrow kink bandwidths (~1 μm), and (3) an average angle, μ, of ~40° between matrix lamellae and lamellae within kink bands. All these observations are in accord with the basic assumption of the theory, i.e., well-defined kink bands at their late stages of evolution. In the analysis section, this shoulder peak corresponding to a substantial population of kink bands will be used to evaluate the dynamics of kink band rotation using the equation developed in the theory section, eq 15.

Figure 5 shows the azimuthal intensity distribution (open symbols) as a function of strain during the forward steady shear at 0.1 s^{-1} from 0 to 80% strain. Five consecutive scans at 20% strain intervals are plotted and shifted vertically between successive strain amplitudes (except for $\gamma = 0$) in this and subsequent figures. An angular range of −60° to 120° is chosen as the azimuthal integration limit in order to satisfy the periodicity of the SAXS data and to avoid the beam stop that partially obscures the second-order reflection. Note that the direction of forward shear, or the vorticity of the flow during forward shear, tends to rotate lamellae to higher μ values.

Two important changes are evident in Figure 5 as the strain increases. The position of the maximum in the main peak (μ_1*) shifts to lower angles ($\mu < 0$) during the forward steady shear. This anti-vorticity shift in the maximum of the main peak has been described previously by a sine-squared "rigid rotation model" for the predominately parallel matrix.[10] More importantly for this study, the shoulder of the main peak that corresponds to the kink band population separates from the main peak and develops into a secondary peak during forward shear (μ_k*). This secondary peak position shifts to higher μ values with increasing strain and narrows. Similar results were observed at 0.01 and 0.001 s^{-1} (Figures 6 and 7). While our previous studies, especially our ex situ electron microscopy results, suggest that lamellae within kink bands rotate during shear deformation,[8] these in situ SAXS data provide the most direct

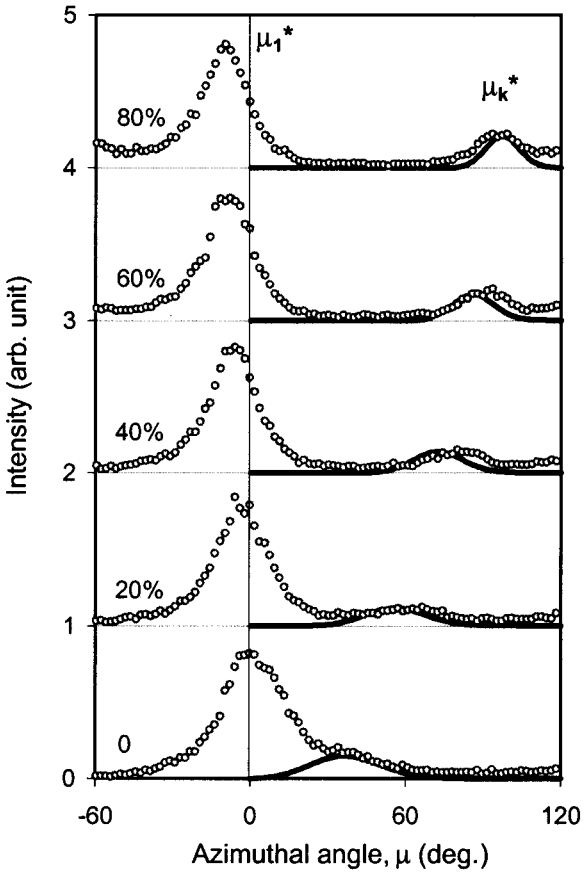

Figure 5. Intensity as a function of azimuthal angle for SEP-(38-62) during steady shear at 180 °C, 0.1 s^{-1}, and up to 80% total strain. Open symbols represent the scattering data at 0−80% strain. At $\gamma = 0$ the solid line represents the fit to the shoulder of the main peak, corresponding to initial kink band population. At γ = 20−80%, the solid line represents the evolution of kink bands according to eq 30. Data were shifted vertically between successive strain amplitudes (except for γ = 0) for clarity in Figures 5−8.

evidence of lamellar rotation within kink bands, as will be shown in the next section.

Analysis

We now compare the predictions of the theory to the scattering data obtained during in situ SAXS-steady shear. We define an orientation probability density $P(\mu,t)$ for kink bands, which is proportional to the volume fraction of the kink band population with orientation μ at time t. We assume that the distribution of orientations within the kink band population evolves solely by rotation of the lamellar normals within the 1−2 plane, according to eq 15, and that there are no changes in kink band width. The evolution of the probability density is thus controlled by a differential conservation equation

$$\frac{\partial P}{\partial t} = -\frac{\partial}{\partial \mu}(\dot{\mu} P) \tag{23}$$

in which the rate of rotation $\dot{\mu} = \dot{\mu}(\mu)$ is given by eq 15. Equation 23 may be solved, given an initial distribution of kink band orientations $P(\mu_0,0)$ at $t = 0$, by requiring that the probability $P(\mu,t)$ that a randomly chosen kink band will have an orientation μ at time t satisfies

$$P(\mu,t)\, \mathrm{d}\mu = P(\mu_0,0)\, \mathrm{d}\mu_0 \tag{24}$$

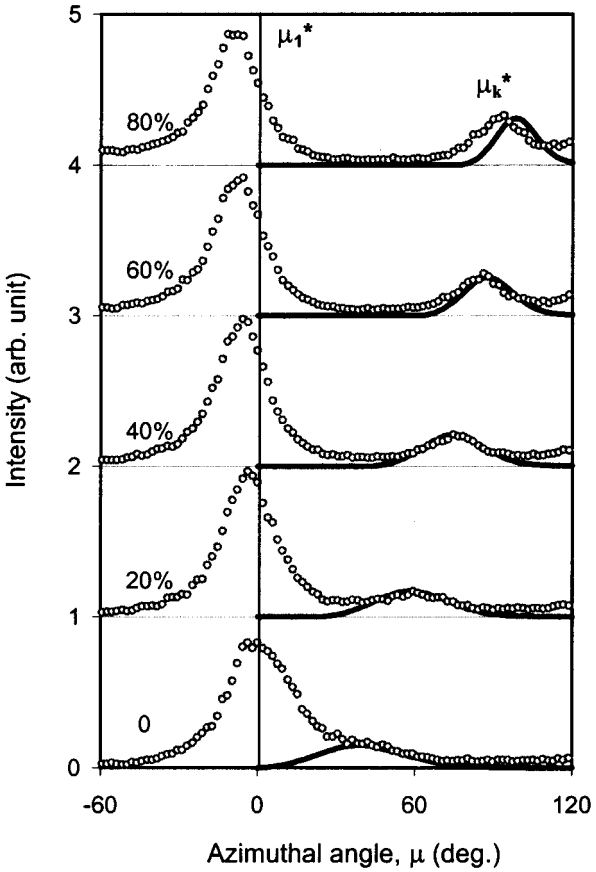

Figure 6. Intensity as a function of azimuthal angle for SEP-(38-62) during steady shear at 180 °C, 0.01 s^{-1}, and up to 80% total strain. Open symbols represent the scattering data at 0−80% strain. At $\gamma = 0$ the solid line represents the fit to the shoulder of the main peak, corresponding to initial kink band population. At γ = 20−80%, the solid line represents the evolution of kink bands according to eq 30.

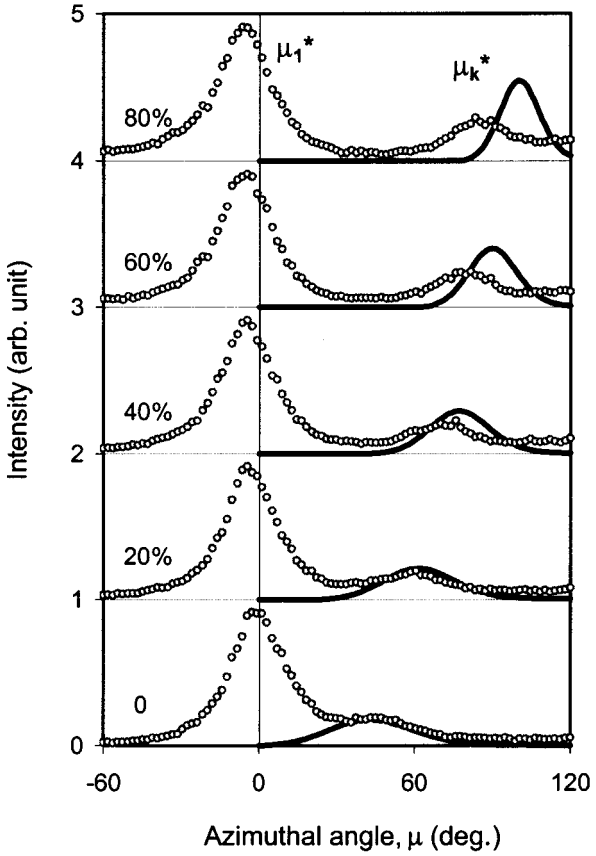

Figure 7. Intensity as a function of azimuthal angle for SEP-(38-62) during steady shear at 180 °C, 0.001 s^{-1}, and up to 80% total strain. Open symbols represent the scattering data at 0−80% strain. At $\gamma = 0$ the solid line represents the fit to the shoulder of the main peak, corresponding to initial kink band population. At $\gamma = 20-80\%$, the solid line represents the evolution of kink bands according to eq 30.

or, equivalently, that

$$P(\mu,t) = P(\mu_0,0)\frac{\partial \mu_0(\mu,t)}{\partial \mu} \tag{25}$$

where $\mu_0(\mu,t)$ is the initial orientation at $t = 0$, expressed as a function of the current orientation and the elapsed time t. Equations 24 and 25 simply require that the probability that a kink band will have an orientation in a range of width dμ around a specified angle μ at time t be equal to the probability that it would have been found in a range of corresponding range dμ_0 of initial orientations around the corresponding initial angle $\mu_0(\mu,t)$, where μ and μ_0 are related by eq 16. By solving eq 16 for μ_0, to obtain

$$\mu_0(\mu,t) = 2\tan^{-1}[\tan(\mu/2) - kt] \tag{26}$$

and differentiating eq 26 to obtain $\partial\mu_0/\partial\mu|_t$, we find a probability density

$$P(\mu,t) = \frac{P(\mu_0,0)}{[\dot\gamma t\cos(\mu/2)]^2 - 2\dot\gamma t\sin(\mu/2)\cos(\mu/2) + 1} \tag{27}$$

where $\mu_0(\mu,t)$ is given by eq 26.

The orientation-dependent scattered intensity from the kink band population, $I(\mu,t)$, for $0 < \mu < \pi$, is assumed to be proportional to the volume fraction of lamellae within kink bands with orientations μ, giving an intensity

$$I(\mu,t) \propto P(\mu,t) \tag{28}$$

in this range of angles. The dynamical model contains only kink bands with orientations in the range $0 < \mu < \pi$, but a kink band with orientation μ will contribute to scattering at both μ and $\mu + \pi$, so as to produce a predicted scattering intensity for which $I(\mu + \pi,t) = I(\mu,t)$. We focus here on fitting the shape of the secondary maximum within the range $0 < \mu < \pi$, for which eq 28 is valid.

To compare the scattering data with the prediction of the theory, we have fit the magnitude of the secondary peak at $t = 0$ and then used eq 24 to evolve I (or P) forward in time. We use an initial distribution of the form

$$I(\mu_0,0) = \lambda\mu_0(\pi - \mu_0)\exp[-\beta(\mu_0 - \alpha)^2] \tag{29}$$

where the parameters α, β, and λ are fit to the initial scattering intensity. The fit to the starting state using the above equation is shown in Figures 5−7, $\gamma = 0$. By combining eqs 27−29, we obtain a predicted scattering

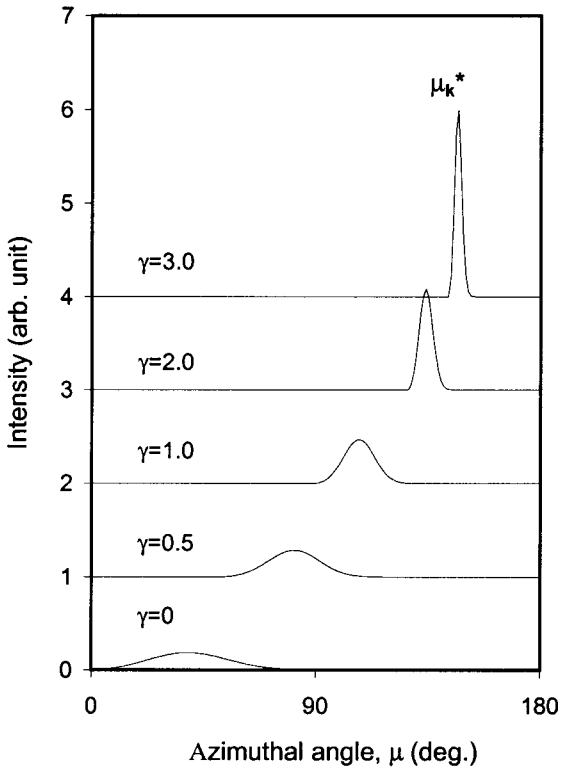

Figure 8. Initial intensity distribution of the kink band population fit by eq 24 and its strain evolution according to eq 30, up to three strain units in total strain.

intensity

$$I(\mu,t) = \frac{\lambda\mu_0(\pi - \mu_0)\exp[-\beta(\mu_0 - \alpha)^2]}{[\dot{\gamma}t\cos(\mu/2)]^2 - 2\dot{\gamma}t\sin(\mu/2)\cos(\mu/2) + 1} \quad (30)$$

Once the values of α, β, and λ are adjusted to fit the initial intensity distribution, the model predicts the evolution of the scattering from the kink bands at all later times, with no adjustable parameters.

Figure 8 shows the predicted time (or strain) evolution of the distribution of kink band orientations up to three strain units. The intensity profiles at different strains are shifted vertically for clarity. The peak moves toward higher μ values with increasing strain. It also sharpens because the rate of rotation of lamellae within kink bands drops monotonically with increasing μ, which causes kink bands in the trailing end of the distribution to rotate faster than those at the leading edge. At very large strains, the orientations of all kink bands are predicted to asymptotically approach π, the double-folded parallel orientation, resulting in a very sharp distribution at this angle. However, our previous electron microscopy study showed that lamellae at the kink band boundary region will not rotate all the way to $\mu = 180°$ but rather break at large-amplitude strains before reaching the parallel orientation (e.g., $\mu \sim 135°$) due to the high free energy associated with such a large angle across the tilt boundary.[8]

Figures 5−7 show the comparison between the SAXS data and the theoretical predictions for steady shear at $\dot{\gamma} = 0.1$, 0.01, and 0.001 s^{-1}, up to 80% total strain. For the fastest shear rate, $\dot{\gamma} = 0.1\ s^{-1}$, the theory accurately predicts the evolution of the peak and correctly predicts both the strain dependence of the peak position and the narrowing of the peak. At lower shear rates of 0.01 and 0.001 s^{-1}, the model still captures qualitative features of the data, but there is a systematic degradation in the quantitative accuracy of the prediction with decreasing shear rate. Specifically, the predicted rate of rotation of the secondary peak is predicted to be faster than that observed in the lower shear rate experiments.

The model predicts that the evolution of the intensity distribution should depend only upon the total macroscopic strain, independent of shear rate or other details of shear history, and thus cannot explain the observed slight differences between the scattering intensities obtained at equal strains but widely disparate shear rates. The fact that the theory most accurately predicts the evolution of the scattering from kink bands at high shear rates suggests that the rigid, reversible rotation of kink bands described by the model may compete with other spontaneous relaxation mechanisms that become more important at lower shear rates.

The SAXS data do not appear to be consistent with the presence of significant changes in kink band width via boundary migration. Any tendency of the two tilt boundaries flanking a kink band to migrate toward each other, thus decreasing the width of the kink band, or away from each other, thus increasing its width, would result in a change of the volume fraction of the kink band regions of the sample, which should cause a corresponding change in the relative magnitudes of the integrated intensities of the main matrix peak and secondary kink band peak seen in the SAXS experiment. In contrast, kink band rotation, with any expression for the rate of rotation $\dot{\mu}$ such as eq 15, should be describable by a differential conservation equation of the form given in eq 23, which rigorously preserves the integrated probability (or intensity) under the kink band peak. An integration of the area under the kink band peak shows no noticeable change in the integrated intensity of the peak; i.e., the area under the peak is approximately conserved at all three shear rates studied.

Our model predicts that if the matrix is not subjected to significant tension (i.e., to a significant negative first normal stress), then the kink band must be under a state of uniaxial tension. This suggests the possibility that tension within the kink bands could cause a measurable dilation of the lamellar spacing within the kink bands. Previous research[15] has shown that application of a macroscopic uniaxial tension to a lamellar phase can cause a measurable dilation of the lamellar spacing. Other studies[9,13] have also shown, however, that shear flow tends to cause a contraction of the lamellar spacing. We also note that we have no direct experimental measure of the state of stress in the matrix material, which is relevant to the interpretation of measurements of the lamellar spacing and which could depend on details of sample history, such as how the sample was loaded into the rheometer. In this study, we have obtained values for the lamellar spacing within both the kink bands and the matrix by examining the second-, fourth-, and fifth-order reflections along the appropriate azimuthal angles as functions of strain. The lamellar period within the kink band is found to remain nearly equal to that of the undeformed material, to within an experimental accuracy of about 1%, while the lamellar period in the matrix is found to contract by 2−3% at the highest shear rate studied.[13] These observations suggest that the tendency of shear flow to cause contraction might be approximately balanced within the kink bands by the tendency of tension to cause dilation.

These data obviously do not, however, allow us to draw any firm conclusions about the state of stress within the kink bands.

Conclusions

This study explores the motion of kink bands in layered liquids such as copolymer melts under steady shear flow, both theoretically and experimentally, by in situ X-ray scattering.

Our model of the evolution of an idealized kink band assumes the existence of narrow parallel boundaries and of a constant lamellar spacing and is believed to be appropriate to describe the late stages in the evolution of kink bands in steady shear flow, after a poorly understood initial stage in which the kink band is formed. Most of our conclusions about the nature of kink motion follow from two simple observations. First, we find on purely geometrical grounds that migration of a tilt boundary in the direction normal to the boundary must be accompanied by an apparent tangential slippage along the boundary, i.e., by a rapid change in the tangential fluid velocity across the boundary, leading to relatively rapid shear flow within the tilt boundary. Second, we find that, in the limit of well-defined tilt bands, in which the boundary width is much less than the kink band width, the tangential forces exerted across the tilt boundary are simply too small to cause slippage at a rate that would lead to significant boundary migration. Together, these observations lead to the conclusion that, in this limit, boundary migration should be negligible. This, in turn, leads to a model of tilt boundary motion in which (i) the tilt band width (measured along the lamellae) is constant, (ii) tilt boundaries rotate like material surfaces in the shear flow of the surrounding matrix, (iii) the lamellae within the kink band rotate as $\dot{\mu} = 2\dot{\gamma}\cos(\mu/2)$, which is simply twice the rate of rotation of the tilt boundaries, (iv) the rate of shear inside a kink band is opposite in sign and equal in magnitude to that in the matrix, and (v) either the kink or the matrix, or both, must be under a state of uniaxial tension.

We have carried out in situ SAXS-steady shear experiments on a lamellar diblock copolymer, SEP(38-62), in a predominately parallel orientation with a significant kink band population. This experiment allows us to directly test the predictions for the rate of kink band rotation, and the prediction that the kink band width should not change, by following the evolution of a secondary peak in the SAXS scattering intensity as a function of the azimuthal angle that arises from scattering from kink bands. Theoretical predictions for the time (or strain) evolution of this peak are in excellent agreement with our SAXS data at the largest shear rate studied, with no free parameters other than those used to fit the initial peak shape. The level of agreement between the theory and experiment gets noticeably worse with decreasing shear rate. The observed slight dependence of the peak position upon strain rate is inconsistent with the prediction that the intensity should evolve in a way that depends only on the total strain and is presumably due to the presence of some spontaneous relaxation mechanisms not accounted for in our model.

The fact that the integrated area under the secondary peak remains approximately constant at all shear rates studied indicates that there is little change in the overall volume fraction of kink bands with time or strain. Previous ex situ microscopy studies have shown that the average width of kink bands is independent of the applied strain. These two pieces of information combine to suggest that the number of kink bands is approximately independent of the applied strain; that is, no significant number of kink bands are formed while shearing the sample with well-defined kink bands. The absence of new kink bands during shear is an implicit assumption of the model and proves to be consistent with our observations.

Our experimental results provide strong evidence for the validity of the model of kink band motion developed here, at least at the highest shear rate studied. This understanding of the dynamics of kink bands during shear alignment may serve as a reference both in guiding theoretical study of defects in lamellar phases of block copolymer melts, and other smectic A materials, and in controlling processing conditions of such layered liquids.

Acknowledgment. This work was done in collaboration with Prof. A. J. Ryan at the University of Sheffield, UK, using the 16.1 beamline at the Daresbury Laboratory. We thank Anthony Gleeson and Nick Terrill for assisting us with beam setup, collimation, and data processing and Ron Larson for a useful conversation. Lei Qiao and Karen I. Winey acknowledge the funding from the NSF-MRSEC program at the University of Pennsylvania. David C. Morse acknowledges partial support from the NSF-MRSEC program at the University of Minnesota.

References and Notes

(1) Gido, S. P.; Thomas, E. L. *Macromolecules* **1994**, *27*, 6137.
(2) Matsen, M. W. *J. Chem. Phys.* **1997**, *107*, 8110.
(3) Villain-Guillot, S.; Netz, R. R.; Andelman, D.; Schick, M. *Physica A* **1998**, *249*, 285.
(4) Alward, D. B.; Kinning, D. J.; Thomas, E. L.; Fetters, L. J. *Macromolecules* **1986**, *19*, 215.
(5) Kinning, D. J.; Thomas, E. L.; Ottino, J. M. *Macromolecules* **1987**, *20*, 1129.
(6) Polis, D. L.; Winey, K. I. *Macromolecules* **1996**, *29*, 8180.
(7) Polis, D. L.; Winey, K. I. *Macromolecules* **1998**, *31*, 3617.
(8) Qiao, L.; Winey, K. I. *Macromolecules* **2000**, *33*, 851.
(9) Pinheiro, B. S.; Winey, K. I.; Hajduk, D. A.; Gruner, S. M. *Macromolecules* **1996**, *29*, 1482.
(10) Polis, D. L.; Smith, S. D.; Terrill, N. J.; Ryan, A. J.; Morse, D. C.; Winey, K. I. *Macromolecules* **1999**, *32*, 4668.
(11) de Gennes, P.-G.; Prost, J. *The Physics of Liquid Crystals*, 2nd ed.; Oxford University Press: New York, 1993.
(12) Polis, D. L.; Winey, K. I.; Ryan, A. J.; Smith, S. D. *Phys. Rev. Lett.* **1999**, *83*, 2861.
(13) Qiao, L.; Winey, K. I. *Macromolecules*, in press.
(14) Bliss, N.; Bordas, J.; Fell, B. D.; Harris, N. W.; Helsby, W. I.; Mant, G. R.; Smith, W.; Towns-Andrews, E. *Rev. Sci. Instrum.* **1995**, *66*, 1311.
(15) Cohen, Y.; Brinkmann, M.; Thomas, E. L. *J. Chem. Phys.* **2001**, *114*, 984.

MA010611R